

# **Eu- and Tb-adsorbed Si<sub>3</sub>N<sub>4</sub> and Ge<sub>3</sub>N<sub>4</sub>: Tuning the colours with one luminescent host**

Cordula Braun,<sup>[a]\*</sup> Liuda Mereacre,<sup>[a]</sup> Zheng Chen,<sup>[b]</sup> Adam Slabon,<sup>[c]</sup>  
David Vincent,<sup>[d]</sup> Xavier Rocquefelte,<sup>[d]</sup> and Jean-François Halet<sup>[e]</sup>

[a] \* Dr. C. Braun, L. Mereacre,  
Karlsruhe Institute of Technology (KIT)  
Institute for Applied Materials (IAM)  
Herrmann-von-Helmholtz-Platz 1,  
D-76344 Eggenstein-Leopoldshafen  
E-mail: [Cordula.Braun@kit.edu](mailto:Cordula.Braun@kit.edu)

[b] Z. Chen,  
Institute of Inorganic Chemistry, RWTH Aachen University,  
Landoltweg 1,  
D-52056 Aachen

[c] Prof. Dr. A. Slabon,  
Department of Materials and Environmental Chemistry,  
Stockholm University,  
Svante Arrhenius väg 16 C,  
106 91 Stockholm, Sweden

[d] D. Vincent, Prof. Dr. X. Rocquefelte,  
Univ. Rennes - CNRS  
Institut des Sciences Chimiques de Rennes, UMR 6226  
35000 Rennes, France

[e] Prof. Dr. J.-F. Halet  
CNRS – Saint-Gobain – NIMS, IRL 3629,  
Laboratory for Innovative Key Materials and Structures (LINK),  
National Institute for Materials Science (NIMS),  
1-1 Namiki, Tsukuba 305-0044, Japan

## Abstract

Phosphor-converted white light-emitting diodes (pc-LEDs) are emerging as an indispensable solid-state light source for the next generation lighting industry and display systems due to their unique properties. Nitrides with their wide-ranging applicability due to their intriguing structural diversity, their auspicious chemical and physical properties represent an essential component in industrial and materials applications.

Here, we present the successful adsorption of Eu and Tb at the grain boundaries of bulk  $\beta$ -Si<sub>3</sub>N<sub>4</sub> and  $\beta$ -Ge<sub>3</sub>N<sub>4</sub> by a succeeding combustion synthesis. The adsorption of europium and terbium and the synergic combination of both resulted in intriguing luminescence properties of all compounds (red, green, orange and yellow). Especially the fact that one host can deliver different colours renders Eu,Tb- $\beta$ -M<sub>3</sub>N<sub>4</sub> (M= Si, Ge) as prospective chief components for future light emitting diodes (LEDs).

For the elucidation of the *RE* adsorption on the electronic properties of  $\beta$ -Si<sub>3</sub>N<sub>4</sub> and  $\beta$ -Ge<sub>3</sub>N<sub>4</sub>, Mott-Schottky (MS) measurements were conducted for the bare and *RE* adsorbed samples. Further insight on the electronic structure of  $\beta$ -Si<sub>3</sub>N<sub>4</sub> and  $\beta$ -Ge<sub>3</sub>N<sub>4</sub> were obtained via density functional theory (DFT) computations.

## *Main*

Phosphor-converted white light-emitting diodes (pc-LEDs) are emerging as an indispensable solid-state light source for the next generation lighting industry and display systems due to their unique properties.<sup>[1,2]</sup>

Doped gallium nitride (GaN) has been the benchmark in the last decades in this domain and has indeed pushed the LED revolution in lighting and displays as a key material. The concept of down-conversion of a GaN-based blue LED, being awarded the Nobel prize in 2014 in physics,<sup>[3–5]</sup> offers the possibility to provide efficient generation of monochromatic, high-colour purity light resulting in a highly efficient warm-white all-nitride phosphor-converted light emitting diode (pc-LED). The combination of the lower energy consumption, high light quality, preservation of colour point stability and long lifetime is one of the key benefits of pc-LEDs, having the potential to reduce global energy consumption in the lighting sector substantially.

Silicon nitride ( $\text{Si}_3\text{N}_4$ ) high performance ceramics are used in numerous applications because of their superior mechanical properties.<sup>[6,7]</sup> The wide-ranging applicability of nitrides and their related (oxo)nitridosilicate family can be ascribed to their significantly extended structural varieties as well as their auspicious chemical and physical properties (very high chemical and thermal stability, very high quantum efficiency, very low thermal quenching).

In particular,  $\text{Eu}^{2+}$ -doped (oxo)nitridosilicates and SiAlONs have been amply studied as important host lattices for phosphor-converted light-emitting diodes (pc-LEDs).<sup>[8–22]</sup>

For instance,  $\text{M}_2\text{Si}_5\text{N}_8:\text{Eu}^{2+}$  (red-orange, 2-5-8 phosphor) and  $\text{MSi}_2\text{O}_2\text{N}_2:\text{Eu}^{2+}$  (yellow-green, 1-2-2-2 phosphor) ( $\text{M} = \text{Ca}, \text{Sr}, \text{Ba}$ ) were significant discoveries in this field. Several Mg-nitridosilicates and nitridoaluminates were also developed as next generation high efficient red emitting phosphor materials with superior luminescence properties.<sup>[23–27]</sup>

The next step in phosphor development is the investigation of novel host materials for narrow-band emitting phosphors to enhance luminous efficacy and improving therefore the quality of light emitting diodes (LEDs) for diverse applications upon doping.

Silicon nitride ( $\text{Si}_3\text{N}_4$ ) materials have been found to meet these requirements due to its rigid lattices with highly covalent network and high thermal stability.<sup>[28,29]</sup> However, looking at the literature indicates that there are only a few investigations concerning rare-earth doped silicon nitride materials. In most cases only Eu- and Tb-doped  $\alpha\text{-Si}_3\text{N}_4$  thin films and nanowires illustrating broad band emission are concerned.<sup>[30–38]</sup> Here we use the expression doping explicitly as this is given in the references.

There are many works in the literature regarding the influence of rare-earth oxides additives often defining the morphology of  $\beta$ -Si<sub>3</sub>N<sub>4</sub> crystallites growing in a multiphase ceramic, thereby affecting its microstructure and mechanical toughness of the ceramic.<sup>[39–46]</sup> Densification additives (e.g, rare-earth (*RE*) oxides) play an important role in the fabrication of silicon nitride-based ceramics. Indeed, the affinity of the *RE* cations to segregate and adsorb on the prismatic planes of the hexagonal grains in  $\beta$ -Si<sub>3</sub>N<sub>4</sub>, exhibiting very anisotropic shapes, is used to develop microstructural features (e.g, the initiation of the  $\alpha$ - $\beta$  transformation and the formation of elongated reinforcing grains) required for particular applications.<sup>[40]</sup>

Phosphors are usually doped with Eu<sup>2+</sup> and only one activator ion is used. Therefore, one host shows one colour. The fact that one host can be doped with several rare-earth activator ions, even at the same time, is absolutely new resulting in the fact that one host can deliver different colours. As well novel is the fact that a pure nitride host material shows green luminescence,<sup>[28,29]</sup> till now this could only be realized by oxynitrides and oxonitridosilicates.<sup>[15,47–50]</sup>

Just recently we demonstrated that the so called “yellow gap” could be closed for bulk GaN via co-doping with europium and terbium.<sup>[28,29]</sup> Co-doping really opens up a multitude of degrees of freedom to customize and adapt a luminescent material to specific needs.

Herein, we experimentally and theoretically examine the adsorption of Eu and Tb at the grain boundaries of  $\beta$ -Si<sub>3</sub>N<sub>4</sub> and  $\beta$ -Ge<sub>3</sub>N<sub>4</sub> and discuss their resulting intriguing luminescence properties. (For  $\beta$ -Si<sub>3</sub>N<sub>4</sub> and  $\beta$ -Ge<sub>3</sub>N<sub>4</sub> adsorbed with europium and/or terbium we would like to introduce the notation Eu,Tb- $\beta$ -M<sub>3</sub>N<sub>4</sub>.) The results indicate that Eu,Tb- $\beta$ -Si<sub>3</sub>N<sub>4</sub><sup>[28]</sup> and as well as Eu,Tb- $\beta$ -Ge<sub>3</sub>N<sub>4</sub><sup>[28]</sup> should be considered as prospective chief components for highly efficient warm-white all-nitride phosphor-converted light emitting diode (pc-LED).

## ***Results***

### ***Structure and composition characterization***

Various synthetic approaches (e.g., low temperature urea-based method) were successfully used to combine  $\beta$ -Si<sub>3</sub>N<sub>4</sub> and  $\beta$ -Ge<sub>3</sub>N<sub>4</sub> (Chempur 99,999%) with MCl<sub>3</sub> · 6 H<sub>2</sub>O or M(NO<sub>3</sub>)<sub>3</sub> · 5H<sub>2</sub>O (M = Eu, Tb). (see Figure 1a and Figs. S1-3).<sup>[28]</sup>

For a comparison of the powder diffraction patterns of Eu- $\beta$ -Si<sub>3</sub>N<sub>4</sub> and Tb- $\beta$ -Si<sub>3</sub>N<sub>4</sub> see Figure S1, for Tb- $\beta$ -Ge<sub>3</sub>N<sub>4</sub> and Eu,Tb- $\beta$ -Ge<sub>3</sub>N<sub>4</sub>, see Figure S3. SEM EDX measurements of  $\beta$ -Si<sub>3</sub>N<sub>4</sub> and  $\beta$ -Ge<sub>3</sub>N<sub>4</sub> confirmed the atomic ratio of M:N (M = Si, Ge) of 3:4 and europium and terbium contents of 3-5% were found.

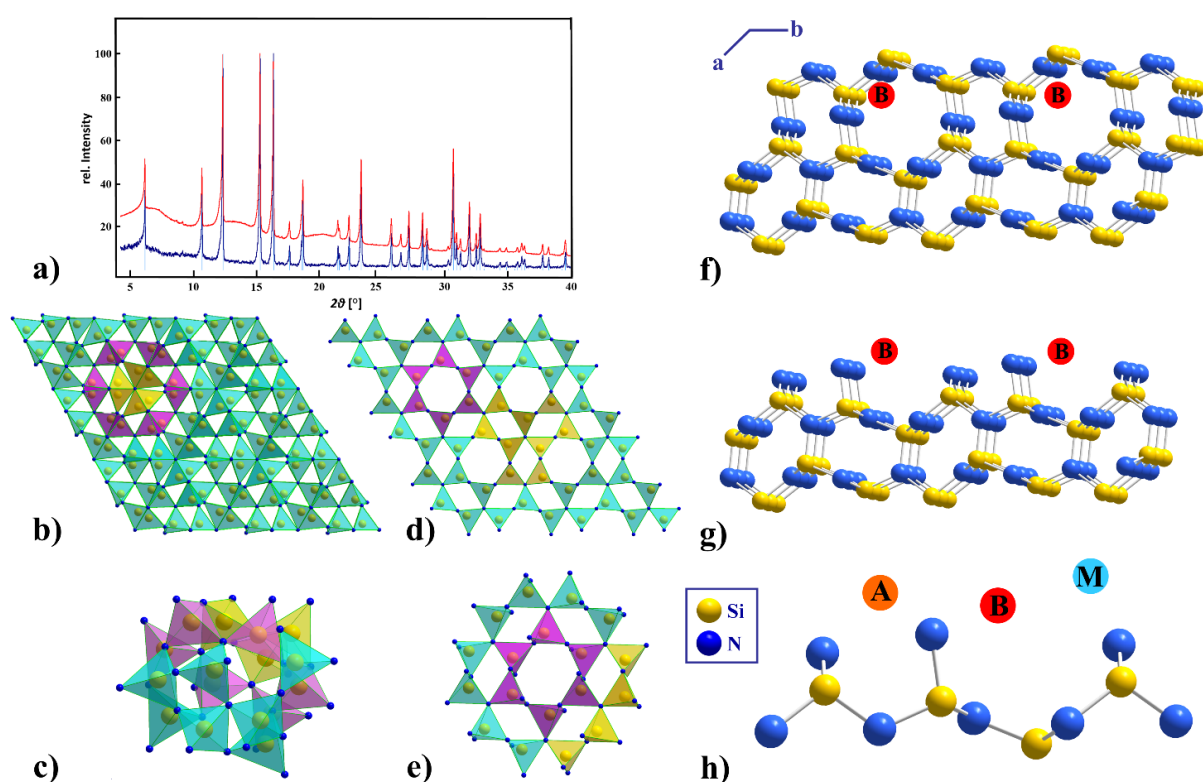


Figure 1: a) X-ray powder diffraction patterns of pure  $\beta$ - $\text{Si}_3\text{N}_4$  (blue), adsorbed Eu- $\beta$ - $\text{Si}_3\text{N}_4$  (red) and the bar graph of  $\beta$ - $\text{Si}_3\text{N}_4$  ICSD [33-1160] (bright blue), ( $\lambda = 0.709026 \text{ \AA}$ ), b) structure of  $\alpha$ - $\text{Si}_3\text{N}_4$  view along [001], c) Cavity for a possible insertion of a *RE* cation in  $\alpha$ - $\text{Si}_3\text{N}_4$ , d) structure of  $\beta$ - $\text{Si}_3\text{N}_4$  view along [001], e) six-ring representation of  $\beta$ - $\text{Si}_3\text{N}_4$ , f), g) and h) structure of  $\beta$ - $\text{Si}_3\text{N}_4$  view along [001] with three possible *RE* adsorption sites A, B, and M.<sup>[41]</sup> (Si atoms are depicted in yellow, N atoms in blue, the *RE* adsorption sites A, B, and M in orange, red and light blue)

Understanding the influence of selective dopant additions and the role of interfacial interactions is central to the design of novel high-performance  $\text{Si}_3\text{N}_4$  ceramics by offering the potential for customizing the materials properties. Rare-earth cations are often located within regions of the oxynitride glassy phase of triple-junction pockets, disordered amorphous nanometer scale intergranular films (IGF) and at the glass or IGF/ $\beta$ - $\text{Si}_3\text{N}_4$  grain interfaces.<sup>[41]</sup>

According to the literature<sup>[41,46]</sup> there are three independent stable *RE* adsorption sites per surface unit cell along the N-terminated prismatic planes of  $\beta$ - $\text{Si}_3\text{N}_4$ . (see Figure 1f, g, h) A and B are stable *RE* equilibrium sites, while calculations pretended the M site to be theoretically unstable, although observed experimentally in the case of La adsorption.<sup>[41]</sup> Stereochemical bonding factors are found to determine the adsorption site preferences contrary to ionic size effects, and the strength of the rare-earth interface bonding is defined inter alia by the electronic structure of the

nitride surface. Shibata *et al.*<sup>[46]</sup> showed that these *RE* adsorption sites have higher binding energies than Si, partially reside on cation sites normally only available for Si and that the *RE*-N bonds are longer than comparable Si-N bonds. While in  $\beta$ - $\text{Si}_3\text{N}_4$  an adsorption of the *RE* ions at the grain boundaries is possible (see Figure 1f,g,h), in  $\alpha$ - $\text{Si}_3\text{N}_4$  an insertion of cations into the structure (see Figure 1c) takes place. In the  $\alpha$ - $\text{Si}_3\text{N}_4$  structure there are two caves (for the bigger one see Figure 1c), which can be occupied when charge is balanced by cation and/or anion substitutions (e.g., Si by Al and N by O). This additional insertion of an *RE* ion is stabilizing the  $\alpha$ - $\text{Si}_3\text{N}_4$ , which is otherwise metastable.<sup>[51]</sup> And indeed, no insertion of cations is realized into the six rings in  $\beta$ - $\text{Si}_3\text{N}_4$ . (see Figure 1e)

## ***Luminescence properties***

One of the most important activator ions with red emission is  $\text{Eu}^{3+}$  corresponding to the transition  $^5\text{D}_0 \rightarrow ^7\text{F}_J$  ( $J = 1-6$ ). For  $\text{Tb}^{3+}$ , the green emission is due to the transition between the  $^5\text{D}_J$  emitting states and the  $^7\text{F}_J$  ground states, where the main intense green emission is attributed to the  $^5\text{D}_4 \rightarrow ^7\text{F}_5$  transition (544 nm).

An important point here is that normally the *RE* ion of luminescent phosphors is inserted during the main synthesis and not afterwards. In general, doping of nitridosilicates is performed with  $\text{Eu}^{2+}$  and only one activator ion is used for one luminescent host. Blending the colours within one host and colour tuning by mixing different coloured luminescent hosts should open up tremendous opportunities for highly efficient phosphors. Within the scope of this work,  $\beta$ - $\text{Si}_3\text{N}_4$  and  $\beta$ - $\text{Ge}_3\text{N}_4$  were adsorbed with Eu and Tb activator ions each individually and both simultaneously.

In the CIE 1931 diagram (see Figure 2c) the chromaticity coordinate positions of Eu- and Tb-  $\beta$ - $\text{Si}_3\text{N}_4$  and  $\beta$ - $\text{Ge}_3\text{N}_4$  are indicated, proving that a colour tuning of one host with different activator ions and their combination is feasible.

Taking into account the basics of colour mixing, it is clear that the combination of green and red leads to orange. (see Figure 2f) This effect could be proven in the meantime for other doped nitrides<sup>[28]</sup> e.g.,  $\text{GaN}$ <sup>[29]</sup> (see Figure 2c), and carbodiimides as well.<sup>[52]</sup>

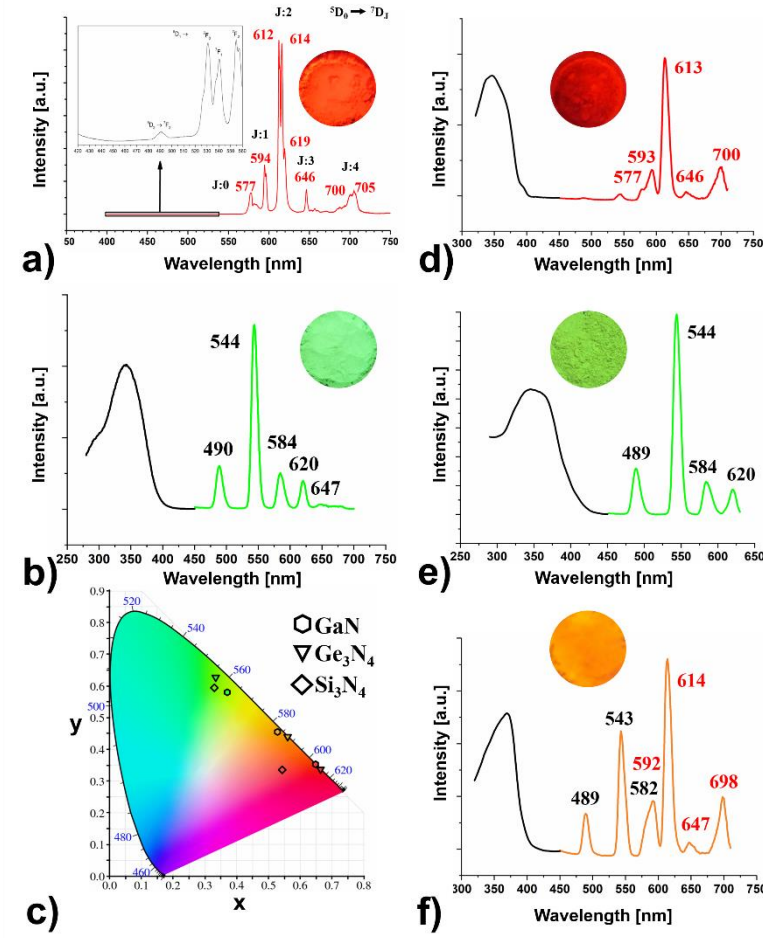


Figure 2: Excitation (black) and emission spectra (coloured) of a) Eu-β-Si<sub>3</sub>N<sub>4</sub> (red), b) Tb-β-Si<sub>3</sub>N<sub>4</sub> (green) and of d) Eu-β-Ge<sub>3</sub>N<sub>4</sub> (red), e) Tb-β-Ge<sub>3</sub>N<sub>4</sub> (green) and f) Eu- and Tb-β-Ge<sub>3</sub>N<sub>4</sub> (orange), c) CIE 1931 diagram of β-Si<sub>3</sub>N<sub>4</sub> (◇), β-Ge<sub>3</sub>N<sub>4</sub> (▽) and GaN (●)<sup>[29]</sup> adsorbed/doped with Eu, Tb and Eu and Tb.

Eu-β-Si<sub>3</sub>N<sub>4</sub> and Eu-β-Ge<sub>3</sub>N<sub>4</sub> show strong characteristic emission peaks of Eu<sup>3+</sup> within the region of 570-705 nm, indicating an energy transfer between the β-Si<sub>3</sub>N<sub>4</sub> and β-Ge<sub>3</sub>N<sub>4</sub> hosts and the Eu<sup>3+</sup> ions. The peaks associated with the intra-4f shell transitions (<sup>5</sup>D<sub>0</sub> → <sup>7</sup>F<sub>J</sub>) of the Eu<sup>3+</sup> ions, are found at 577, 594, 612, 614, 619, 646 and 700, 705 nm, with those at 612 and 614 nm the most intense ones for β-Si<sub>3</sub>N<sub>4</sub> (see Figure 2a) whereas for Ge<sub>3</sub>N<sub>4</sub>, the corresponding peaks are located at 577, 593, 613 (the most intense), 646 and 700 nm (see Figure 2d).

Figure 2a shows that in the emission spectrum of Eu-β-Si<sub>3</sub>N<sub>4</sub>, the transitions <sup>5</sup>D<sub>0</sub> → <sup>7</sup>F<sub>0</sub> and <sup>7</sup>F<sub>3</sub> seem to be more intense than usually, and the latter is even more pronounced than the <sup>5</sup>D<sub>0</sub> → <sup>7</sup>F<sub>4</sub> transition, which is not common. This means a strong *J*-mixing and a strong crystal-field

perturbation might occur in this matrix. The peak corresponding to the  $^5D_0 \rightarrow ^7F_0$  transition is also broad, indicating the location of  $Eu^{3+}$  ions on several sites in the host structure. (see Figure 2a)

The excitation (monitored at 544 nm) and emission spectra of Tb- $\beta$ - $Si_3N_4$  and Tb- $\beta$ - $Ge_3N_4$  are represented in Figure 2b and e. The excitation spectrum of Tb- $\beta$ - $Si_3N_4$  and Tb- $\beta$ - $Ge_3N_4$  exhibit a broad and intense band in the range from 280 nm to 380 nm with peaks at around 342 and 356 nm, respectively. This broad band is attributed to  $4f^8 \rightarrow 4f^7 5d^1$  transition of the  $Tb^{3+}$  ions. The strongest emission peak is at 544 nm with a full width at half maximum (FWHM)  $\sim 12$  nm corresponding to the  $^5D_4 \rightarrow ^7F_5$  transition, while the peaks at 488, 489 nm, 584 nm and 620 nm originate from the  $^5D_4 \rightarrow ^7F_6$ ,  $^5D_4 \rightarrow ^7F_4$  and  $^5D_4 \rightarrow ^7F_3$  transitions of the  $Tb^{3+}$  ions, respectively. The green luminescence of Tb- $\beta$ - $Si_3N_4$  and Tb- $\beta$ - $Ge_3N_4$  demonstrates impressively that green emitting phosphors<sup>[28]</sup> can be also achieved with purely nitride compounds and not only with oxynitrides (e.g.,  $\beta$ -SiAlON:Eu<sup>2+</sup><sup>[53]</sup>) or oxonitridosilicates (e.g., SrSi<sub>2</sub>O<sub>2</sub>N<sub>2</sub>:Eu<sup>2+</sup><sup>[54,55]</sup>) as it was up to now. The energy level distributions of  $Tb^{3+}$  and  $Eu^{3+}$  ions show a large overlap and their energy transfer has been proven to be very effective.<sup>[56]</sup> The blue-green light of the  $Tb^{3+}$  transition ( $^5D_4 \rightarrow ^7F_{6,5}$ ) is emitted by polychromatic relaxation and the energy is transferred to the  $^5D_1$  and  $^5D_0$  levels of the  $Eu^{3+}$  by cross relaxation. The  $Eu^{3+}$  ions absorbing the energy from  $Tb^{3+}$  emit therefore orange light.

Figure 2f and c proves that for Eu,Tb- $Ge_3N_4$  two different activator ions can be adsorbed in one host showing the typical bands of  $Eu^{3+}$  as well as the ones of  $Tb^{3+}$  in one spectrum resulting in a saturated orange body colour. However, this is not only a superposition of the  $Eu^{3+}$ - and the  $Tb^{3+}$ -spectrum of  $\beta$ - $Ge_3N_4$  because peak form, intensity and wavelength of this orange spectrum differ clearly in comparison to the spectra of the single doped materials. Therefore, this orange colour is only possible by mixing the ions at an atomic scale and cannot be realized simply by a mixture of particles of the red and the green adsorbed  $Ge_3N_4$ .

To get further evidence powder samples of Eu- $Ge_3N_4$  and Tb- $Ge_3N_4$  (same molar ratio Eu:Tb as in Eu,Tb- $Ge_3N_4$ ) were mixed in a mortar. This definitely did not result in an orange luminescent  $\beta$ - $Ge_3N_4$  sample but a yellow luminescent powder instead. (see Figure S4c,d) Indeed, compared to a superposition of the Eu- and Tb-spectra, all peaks of the Eu,Tb- $\beta$ - $Ge_3N_4$  spectrum slightly changed in energy and intensity with the peaks resulting from  $Tb^{3+}$  significantly stronger and tuning the colour to the yellow region (CIE coordinates  $x, y = 0.456, 0.499$ ). This clearly evidenced that the orange body colour (CIE values  $x, y = 0.559, 0.438$ ) can only be obtained by an atomic scale mixing and that we are able to tune the colour resulting finally in red, green, orange and yellow luminescence for Eu- and Tb- $\beta$ - $Ge_3N_4$ . As the mixing at the atomic scale for Eu,Tb- $\beta$ - $Si_3N_4$



was not successful, the combination of the powder samples of equal parts of Eu- $\beta$ -Si<sub>3</sub>N<sub>4</sub> and Tb- $\beta$ -Si<sub>3</sub>N<sub>4</sub> was tested. Here we got a completely different result and the CIE diagram shows a saturated orange colour with the coordinates  $x, y = 0.570, 0.417$ . (see Figure S4a,b) Here we find nearly the same CIE values as the ones of the amber emitting 2-5-8 nitridosilicate phosphor (Ba,Sr)<sub>2</sub>Si<sub>5</sub>N<sub>8</sub>:Eu<sup>2+</sup> ( $x, y = 0.579, 0.416$ ) being considered as an important breakthrough for bridging the “yellow gap”.<sup>[22]</sup>

For Eu,Tb- $\beta$ -Ge<sub>3</sub>N<sub>4</sub> the FWHM pointed out the same value as those of the single doped materials which are in the range of 11-12 nm. This holds true for Tb- $\beta$ -Si<sub>3</sub>N<sub>4</sub> as well. A much more narrow band is observed for Eu- $\beta$ -Si<sub>3</sub>N<sub>4</sub> with a FWHM of 2-4 nm. Interestingly, these values are quite smaller than the line widths (FWHM) of the emission spectra of the very narrow-band nitridosilicate phosphors which range between 35-50 nm,<sup>[2]</sup> or those of the nitride-based LEDs which vary typically between 20-35 nm.<sup>[57]</sup>

To elucidate if the luminescence does not result from the respective rare-earth (*RE*) compounds and if the Eu and Tb ions really have been adsorbed at the grain boundaries of  $\beta$ -Si<sub>3</sub>N<sub>4</sub> and  $\beta$ -Ge<sub>3</sub>N<sub>4</sub> a comparison of the luminescence spectra of Eu-Si<sub>3</sub>N<sub>4</sub> and Ge<sub>3</sub>N<sub>4</sub> and EuCl<sub>3</sub>  $\times$  6 H<sub>2</sub>O is shown in Figure S5 and S6. A comparison between Tb- $\beta$ -Si<sub>3</sub>N<sub>4</sub> and TbOCl<sup>[58]</sup> is also shown in Figure S14. Optical and luminescence spectra are highly sensitive to structural deformation of the nearest environment of *RE* ions. Therefore, it becomes clearly evident here that the emission spectrum has changed due to the adsorption of the Eu cations into the  $\beta$ -Si<sub>3</sub>N<sub>4</sub> and  $\beta$ -Ge<sub>3</sub>N<sub>4</sub> structures.

A very detailed comparison of our results with those of several Eu- and Tb-Si<sub>3</sub>N<sub>4</sub> thin films and nanowires and possible side products published in the literature was carried out. (see supplement Figures S7-14 and corresponding section) This indicated that if some luminescence spectra may seem very similar overall at first sight, it turns out that definitely some changes are observed.<sup>[30][31][32][33][34][35][36][37][38]</sup>

## ***DFT calculations***

The underlying structure-property relationships in a phosphor, i.e., the relationship between, the nature of the specific atoms, their coordination environment, and the density of states are largely determined by its electronic structure.<sup>[59]</sup> Therefore, DFT calculations were carried out to further elucidate the adsorption of *RE* ions at the grain boundaries.

The  $\beta$ -Si<sub>3</sub>N<sub>4</sub> models were generated in such a way to reproduce the interface observed in high-angle annular dark-field STEM (HAADF-STEM) images of *RE* doped Si<sub>3</sub>N<sub>4</sub> by Ziegler *et al.*,<sup>[60]</sup> which evidenced a grain orientated along the [0001] zone axis with the prismatic plane of Si<sub>3</sub>N<sub>4</sub> facing the amorphous intergranular phase. In particular, the rare earth elements have been observed sitting on two atomic sites at the interface, labeled A and B, which are, respectively, small and large open hexagonal rings. (see Figure 3)

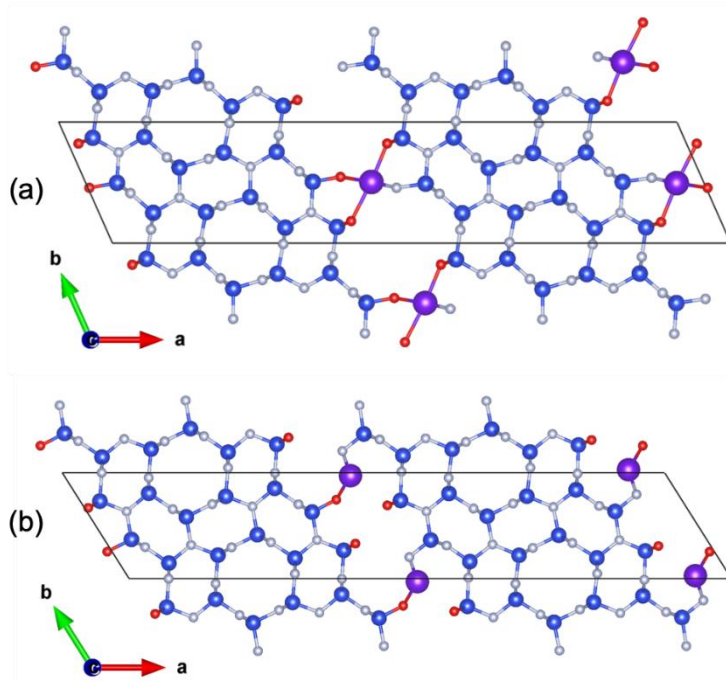


Figure 3: Relaxed atomic structure for the models used to describe the  $\beta$ -Si<sub>3</sub>N<sub>4</sub> grain interface with *RE* elements (Eu or Tb) at the A-site (a) and B-site (b). Nitrogen, oxygen, hydrogen and *RE* atoms are represented in blue, red, white and purple, respectively.

Note that the creation of the interface led to dangling bonds, which were passivated using both O<sup>2-</sup> and N<sup>3-</sup> ions, in order to respect the electroneutrality of the unit cell. For both Eu and Tb ions on sites A and B, atomic coordinates were relaxed leading systematically to a higher stability when the rare earth resides on site A (highly coordinated) than on site B, with an energy difference of 745 and 851 meV per rare earth for Eu<sup>3+</sup> and Tb<sup>3+</sup>, respectively.

For the more stable interface, i.e., with the rare earth located on site A, simulations of the Si *L*<sub>23</sub> edge were performed for silicon atoms close to the interface in order to probe both their location and chemical environment. Indeed, precise electron energy loss spectroscopy (EELS) measurements were reported for *RE* doped Si<sub>3</sub>N<sub>4</sub> ceramics<sup>[60]</sup>, allowing us to compare our model with experimental data. Such a simulation required to properly treat the electron-hole interaction

(excitonic effects) using Bethe-Salpeter equations for instance. Here, due to the size of the system, we chose to consider this electron-hole Coulomb interaction as a static screening using the core-hole approximation. More precisely, half an electron was removed from a core orbital, i.e., the Slater's transition state.<sup>[61]</sup> For the doped Tb- $\beta$ -Si<sub>3</sub>N<sub>4</sub> model, the core-hole was introduced in the  $2p^{1/2}$  and  $2p^{3/2}$  states of the excited silicon atoms. The simulation is thus a summation of two spectra resulting from two static calculations with, respectively, half a core-hole in  $2p^{1/2}$  and  $2p^{3/2}$  states of the probed silicon atoms. In order to validate such a static screening approximation, the related bulk system Si<sub>2</sub>N<sub>2</sub>O was simulated and compared to experiments.<sup>[60]</sup> (see Figure 4a) A good agreement is observed, with a small discrepancy around 104 eV both in terms of peak position and intensity. Such an agreement confirms that the Slater's transition state allows to properly describe the Si  $L_{23}$  edge of silicon atoms surrounded by nitrogen and oxygen atoms.

Figure 4b shows two simulations corresponding to Si  $L_{23}$  edge of two silicon atoms nearby the interface with Tb<sup>3+</sup> ions on site A. One silicon atom, labeled Si<sub>1</sub> (Figure 4b) is surrounded only by nitrogen atoms while the other one, labeled Si<sub>2</sub> (Figure 4b) is environed by oxygen and nitrogen atoms. Note that the experimental spectrum (open circles) related to site A is characterized by a double peak (102 and 103.5 eV), with a first peak assigned to Si-N bonds and the second one to Si-O bonds. Interestingly, our simulations evidenced a peak at 103 eV for Si<sub>1</sub> and 104.1 eV for Si<sub>2</sub>, confirming the previous interpretation and validating the model used to mimic locally the interface in the grain boundary region.

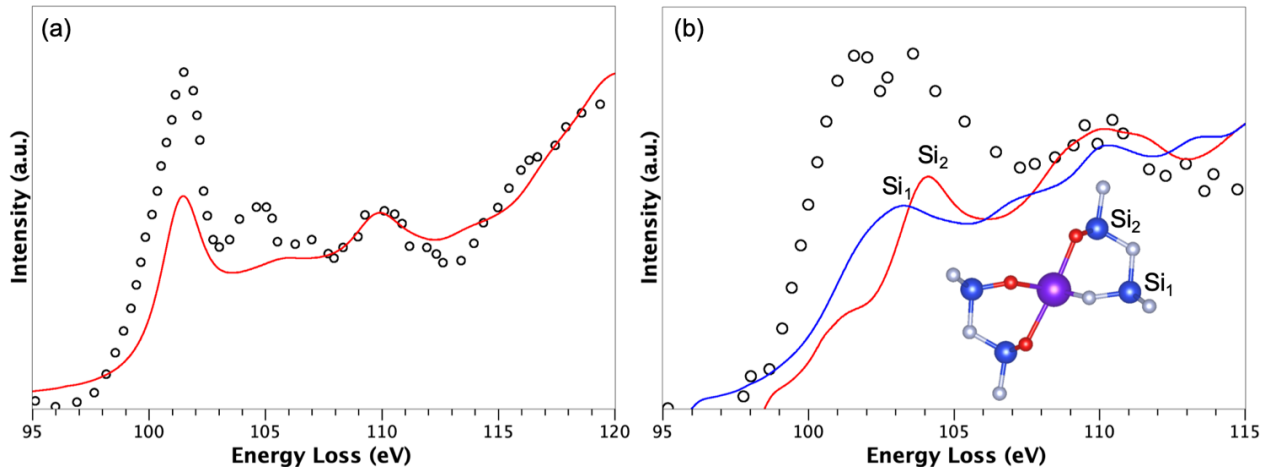


Figure 4: Simulated Si  $L_{23}$  EELS data (red and blue lines) compared to measurements (open circles) from ref.<sup>[60]</sup> of (a) Si<sub>2</sub>N<sub>2</sub>O and (b) the doped Tb- $\beta$ -Si<sub>3</sub>N<sub>4</sub> model with Tb ions on A site. The simulations have been done using the Slater's transition state. For the interface, two simulations have been done for one silicon atom surrounded by N<sup>3-</sup> ions only, and one silicon atom with O<sup>2-</sup> ions in its first coordination sphere.

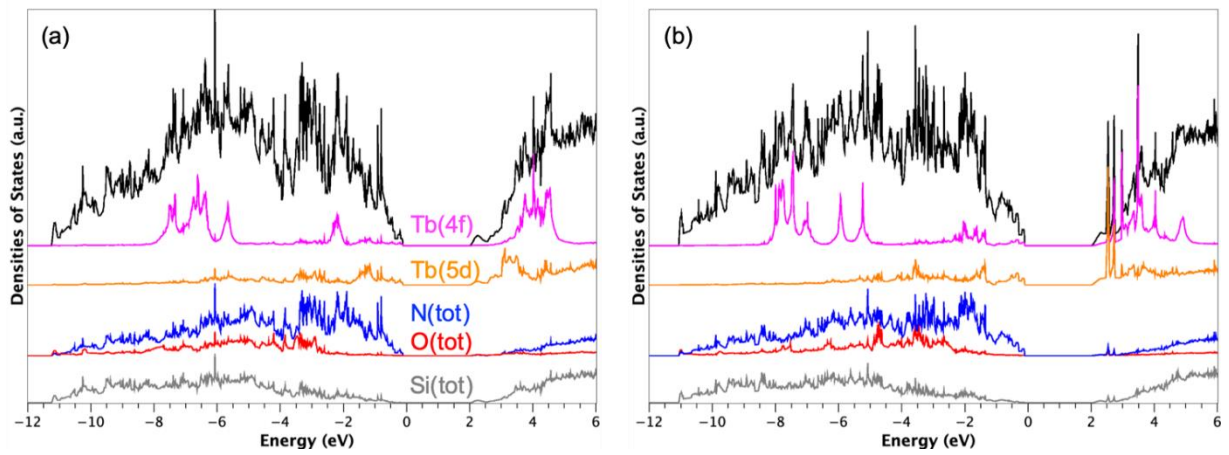


Figure 5: Densities of states (DOS) calculated with Tb atoms on site A (a) and on site B (b). The Fermi level was defined as the reference of energies ( $E_F = 0$  eV). The total DOS is represented in black and the projected DOS in colours. The calculations were carried out at the DFT+U+SOC level of theory, i.e., with  $U_{\text{eff}} = U - J = 6$  eV for the 4f states of the rare-earth element and including spin-orbit coupling (SOC).

DFT+U+SOC calculations were then carried out on the doped Tb- $\beta$ -Si<sub>3</sub>N<sub>4</sub> model considering the previously optimized atomic structures. Such calculations were indeed not trivial and could be difficult to converge when the ground state is close in energy to other magnetic states. The convergence of these calculations was achieved only for the Tb compounds. Spin (orbital) moments of 6.03 (1.45) and 6.04 (2.73)  $\mu_B$  were computed for Tb ions on sites A and B, respectively, leading to total magnetic moments of 7.48 and 8.77  $\mu_B$ , respectively. These values are somewhat smaller than the theoretical value of 9  $\mu_B$  expected for a free Tb<sup>3+</sup> ion. This is due to the crystalline field of the surrounding ligands which is stronger for Tb ions on site A than on site B. On site A, the most energetically preferred site of Tb is positioned in an octahedral environment, while on site B, Tb is sitting in a too large site, which creates a less intense crystalline field. This explains the weaker moment value, in particular the orbital moment of the former with respect to the latter.

Figure 5 shows the densities of states (DOS) obtained with Tb<sup>3+</sup> atoms on A and B sites computed at the DFT+U+SOC level of theory. The valence band (VB), from -12 to 0 eV, is mainly based on N2p states interacting with Si(3p) states. The O2p states of the interface appears in the VB from -10 to -2 eV. The conduction band, starting at 2 eV, is mainly composed of Si3p states interacting with N2p states. The band gap is only 2 eV in both cases. For comparison, the DFT estimated band gap of  $\beta$ -Si<sub>3</sub>N<sub>4</sub> was 4.2 eV. The decrease in the band gap value is indeed the consequence to

additional interactions involving the Tb5d states found both at the top of the VB and the bottom of the conduction band (CB) (see Figure 5).

Such a band gap reduction was already discussed by Huang *et al.*<sup>[37]</sup> for Y-doped Si<sub>3</sub>N<sub>4</sub>, due to Y4d states. These reduced band gaps are directly responsible for the luminescent properties of the doped  $\beta$ -Si<sub>3</sub>N<sub>4</sub>:RE<sup>3+</sup> (RE = Eu, Tb) materials.

## ***Mott-Schottky (MS) measurements***

The emission colour of a phosphor strongly depends on the nature of the incorporated activator, the host material and its electronic configuration.<sup>[62–65]</sup> Electrochemical impedance spectroscopy (EIS) is an appropriate tool to study ion diffusion and to resolve the chemical identity of the charge carriers by the use of blocking electrodes. Mott-Schottky (MS) measurements are very sensitive to probe changes in the electronic band structure, i.e. charge carrier density, type of semiconducting behaviour and band edge positions, upon adsorbing. For the elucidation of the adsorbing effect on the electronic properties of Si<sub>3</sub>N<sub>4</sub> and Ge<sub>3</sub>N<sub>4</sub>, MS measurements were conducted for the bare and RE doped samples. They were performed in a 0.1 M potassium phosphate electrolyte (pH 7) in the dark with a setting at ac amplitude of 5 mV and at an applied frequency of 10, 100 and 1000 Hz. (see Figures S15, S16). As shown in Figure 6, all of the acquired curves show a positive slope corresponding to the characteristic of n-type semiconductors, indicating that bare and RE doped materials of  $\beta$ -Si<sub>3</sub>N<sub>4</sub> and  $\beta$ -Ge<sub>3</sub>N<sub>4</sub> are n-type semiconductors.<sup>[66]</sup> In addition, a smaller slope for all curves can be attributed to increased charge carrier density for Si<sub>3</sub>N<sub>4</sub> upon adsorbing with the rare-earth metals.<sup>[67,68]</sup> The extrapolation of the curves allows to estimate the flat band potential as the corresponding conduction band edge of n-type semiconductors. A comparison of the results obtained from these plots in Figure 6 reveals that the obtained conduction band edges of RE adsorbed Si<sub>3</sub>N<sub>4</sub> and Ge<sub>3</sub>N<sub>4</sub> yield a significant shift, indicating that RE adsorbing can be applied to modify the (photo)electrochemical properties of Si<sub>3</sub>N<sub>4</sub> and Ge<sub>3</sub>N<sub>4</sub>.<sup>[68–70]</sup>

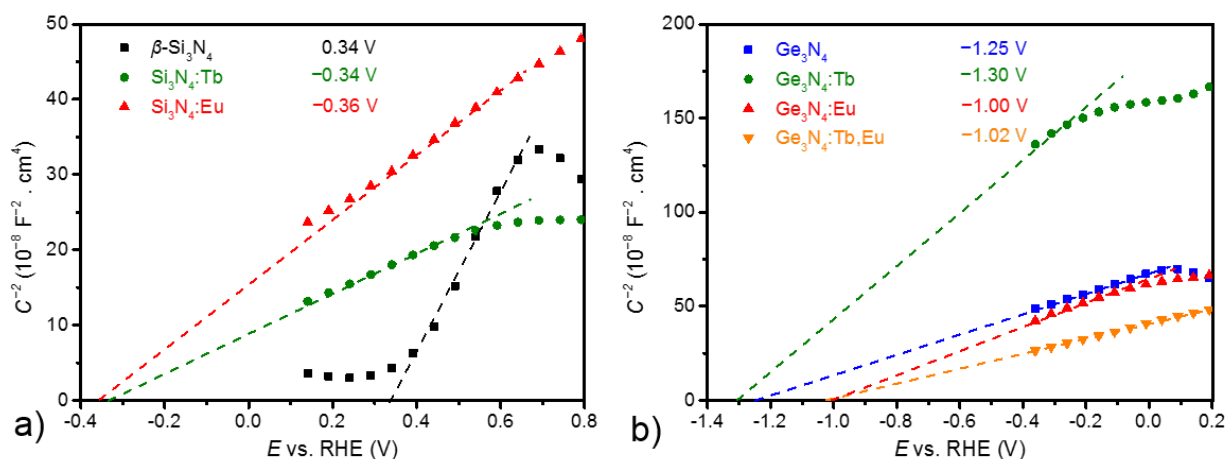


Figure 6: MS analysis of EIS measurements of a) pure  $\text{Si}_3\text{N}_4$  (black),  $\text{Tb-Si}_3\text{N}_4$  (green),  $\text{Eu-Si}_3\text{N}_4$  (red) and b) pure  $\text{Ge}_3\text{N}_4$  (blue),  $\text{Tb-Ge}_3\text{N}_4$  (green),  $\text{Eu-Ge}_3\text{N}_4$  (red) and  $\text{Eu,Tb-Ge}_3\text{N}_4$  (orange). Measurements were performed in a 0.1 M potassium phosphate electrolyte at pH 7, at an applied frequency of 100 Hz for a) and an applied frequency of 1000 Hz for b). The extrapolated curves at  $y = 0$  correspond to the conduction band edges, because the materials exhibit a positive slope that is characteristic for an n-type semiconductor. The determined flatband potentials are provided in the inset.

## Conclusions

The successful adsorption of bulk  $\beta\text{-Si}_3\text{N}_4$  and  $\beta\text{-Ge}_3\text{N}_4$  with Eu and Tb and the synergic combination of both resulted in intriguing luminescence properties of all adsorbed compounds (red, green, orange and yellow). The theoretical and experimental results strongly highlight the opportunities for controlling functionality and luminescence properties of modern energy-efficient white light-emitting diodes.

Especially, the fact that one host can deliver different colours renders  $\text{Eu,Tb-Si}_3\text{N}_4$  and  $\text{Eu,Tb-}\beta\text{-Ge}_3\text{N}_4$  as prospective chief components for future light emitting diodes (LEDs). Not only several colours could indeed be realized by an atomic scale mixing, but the colour could also be tuned by mixing the adsorbed hosts enlarging the colour range with red, green, orange and yellow luminescence for the extremely narrow-band Eu- and Tb- $\text{M}_3\text{N}_4$  materials ( $\text{M} = \text{Si, Ge}$ ). It could be shown that the realization of an amber emitting phosphor for both,  $\text{Si}_3\text{N}_4$  and  $\text{Ge}_3\text{N}_4$ , is possible. This work also studied the types and the flat band edges of  $\beta\text{-Si}_3\text{N}_4$  and  $\beta\text{-Ge}_3\text{N}_4$  before and after adsorption with RE materials were also studied in this work. A detailed physical characterization by MS analysis of EIS revealed that a significant shift of the flat band edge was observed caused by the adsorbing with Eu and Tb ions. This can be seen as a complementary strategy to modify the

band edge of materials. Moreover, this could be applicable to photoelectrodes used to adapt and optimize (photo)electrochemical performances.

## ***Experimental Section***

### **Adsorption of Si<sub>3</sub>N<sub>4</sub> and Ge<sub>3</sub>N<sub>4</sub>:**

The adsorption of  $\beta$ -Si<sub>3</sub>N<sub>4</sub> (Chempur 99,999%) and  $\beta$ -Ge<sub>3</sub>N<sub>4</sub> (VWR 99,99%) was realized by a successive combustion synthesis in combination with the respective metal chlorides (MCl<sub>3</sub>·6 H<sub>2</sub>O or M(NO<sub>3</sub>)<sub>3</sub>·5H<sub>2</sub>O (M= Eu, Tb), NH<sub>4</sub>NO<sub>3</sub>, urea and H<sub>2</sub>O. This mixture was put into an oven for 10 min at 400-600°. The *RE* content, which is about 3-5 at.%, -has been checked via EDX measurements.

### ***X-ray diffraction***

X-ray diffraction experiments on Si<sub>3</sub>N<sub>4</sub>- and Ge<sub>3</sub>N<sub>4</sub>-based powder samples were performed on a STOE STADI P powder diffractometer in Debye-Scherrer geometry with Ge (111)-monochromatized Mo-*K* $\alpha_1$  radiation ( $\lambda = 0.709026$  Å). The samples were enclosed in a glass capillary of 0.3 mm diameter.

### ***EDX measurements***

SEM was performed on a Zeiss Merlin microscope and for EDX we used a Quantax 400 system from Bruker.

## ***Mott-Schottky (MS) measurements***

### **Electrodes fabrication**

Si<sub>3</sub>N<sub>4</sub> and Ge<sub>3</sub>N<sub>4</sub> and the corresponding rare-earth metal (*RE*= Eu, Tb and Eu/Tb) adsorbed semiconductor electrodes were prepared by electrophoretic deposition. Fluorine doped tin oxide (FTO) glass (2.2 mm thick, Sigma-Aldrich) was used as the substrate after sequentially ultrasonic cleaning with dilute nitric acid, acetone and ethanol for 15 min. The dispersion was prepared by mixing 5 mg iodine and 20 mg sample with 20 ml acetone, followed by treatment with ultrasounds. The electrodes were obtained after depositing the dispersed powder at 30 V and drying under ambient atmosphere.

### **Mott-Schottky (MS) measurements**

The MS measurements were performed in an electrochemical cell using a potentiostat (Gamry instruments) operating in a three-electrode setup. The deposited samples on FTO, a 1 M Ag/AgCl electrode and a platinum wire were used as a working electrode, a reference electrode and a counter electrode, respectively. All MS data were recorded vs.  $E_{1\text{ M Ag/AgCl}}$  (V), which was subsequently converted with respect to  $E_{\text{RHE}}$  (V) according to the formula:  $E_{\text{RHE}}$  (V) = 0.235 +  $E_{1\text{ M Ag/AgCl}}$  +  $[0.059 \times \text{pH}]$  (V) at 25 °C.

### ***Luminescence***

The luminescence spectra and quantum yield measurements were performed on a Fluorolog®-3 Horiba Jobin Yvon equipped with a TBX detector picosecond photon detection device and a 450 W xenon lamp.

### ***DFT calculations***

Density functional theory (DFT) calculations were carried out on pure and adsorbed  $\beta\text{-Si}_3\text{N}_4$  and  $\beta\text{-Ge}_3\text{N}_4$ . See supplement for the computational details.

### ***Acknowledgement***

The authors gratefully acknowledge Udo Geckle (IAM-ESS KIT Karlsruhe) for the EDX and Sabine Schlabach (INT KIT Karlsruhe) for luminescence measurements.



## References

- [1] P. Ball, *Nat. Mater.* **2015**, *14*, 453–453.
- [2] P. Pust, P. J. Schmidt, W. Schnick, *Nat. Mater.* **2015**, *14*, 454–458.
- [3] S. Nakamura, *Angew. Chem. Int. Ed. Engl.* **2015**, *54*, 7770–7788.
- [4] I. Akasaki, *Angew. Chem. Int. Ed. Engl.* **2015**, *54*, 7750–7763.
- [5] H. Amano, *Angew. Chem. Int. Ed. Engl.* **2015**, *54*, 7764–7769.
- [6] M. Zeuner, S. Pagano, W. Schnick, *Angew. Chem. Int. Ed. Engl.* **2011**, *50*, 7754–7775.
- [7] H. Lange, G. Wötting, G. Winter, *Angew. Chem. Int. Ed. Engl.* **1991**, *30*, 1579–1597.
- [8] C. Braun, Neue Hochdruckphasen Der Nitrido- und Oxonitridosilicate und verwandter binärer Nitride, doctoral thesis, Ludwig-Maximilians-Universität München, **2010**.
- [9] S. R. Römer, C. Braun, O. Oeckler, P. J. Schmidt, P. Kroll, W. Schnick, *Chem. Eur. J.* **2008**, *14*, 7892–7902.
- [10] T. Jüstel, H. Nikol, C. Ronda, *Angew. Chem. Int. Ed. Engl.* **1998**, *37*, 3084–3103.
- [11] C. Ronda, Ed. , *Luminescence*, Wiley-VCH Verlag GmbH & Co. KGaA, Weinheim, Germany, **2007**.
- [12] W. Schnick, *Phys. Status Solidi - Rapid Res. Lett.* **2009**, *3*, 1–2.
- [13] P. Schmidt, A. Tuecks, J. Meyer, H. Bechtel, D. Wiechert, R. Mueller-Mach, G. Mueller, W. Schnick, *Seventh Int. Conf. Solid State Light.* **2007**, 6669, P6690–P6690.
- [14] K. Uheda, K. Uheda, S. Shimooka, S. Shimooka, M. Mikami, M. Mikami, H. Imura, H. Imura, N. Kijima, N. Kijima, *Sci. Technol.* **n.d.**, 899–902.
- [15] C. Braun, M. Seibald, S. L. Börger, O. Oeckler, T. D. Boyko, A. Moewes, G. Miehe, A. Tücks, W. Schnick, *Chem. - A Eur. J.* **2010**, *16*, 9646–9657.
- [16] C. Braun, S. L. Börger, T. D. Boyko, G. Miehe, H. Ehrenberg, P. Höhn, A. Moewes, W. Schnick, *J. Am. Chem. Soc.* **2011**, *133*, 4307–4315.
- [17] C. Braun, H. Ehrenberg, W. Schnick, *Eur. J. Inorg. Chem.* **2012**, *2012*, 3923–3928.
- [18] R. Mueller-Mach, G. Mueller, M. R. Krames, H. A. Höppe, F. Stadler, W. Schnick, T. Juestel, P. Schmidt, *Phys. Status Solidi A* **2005**, *202*, 1727–1732.
- [19] Y. Q. Li, G. de With, H. T. Hintzen, *J. Mater. Chem.* **2005**, *15*, 4492–4496.
- [20] X. Piao, T. Horikawa, H. Hanzawa, K. Machida, *Appl. Phys. Lett.* **2006**, *88*, 161908-1-161908–3.
- [21] R. J. Xie, N. Hirosaki, Y. Li, T. Takeda, *Materials (Basel)*. **2010**, *3*, 3777–3793.
- [22] R. Mueller-Mach, G. O. Mueller, M. R. Krames, O. B. Shchekin, P. J. Schmidt, H. Bechtel, C. H. Chen, O. Steigermann, *Phys. Status Solidi - Rapid Res. Lett.* **2009**, *3*, 215–217.
- [23] S. Schmiechen, H. Schneider, P. Wagatha, C. Hecht, P. J. Schmidt, W. Schnick, *Chem.*

*Mater.* **2014**, 26, 2712–2719.

- [24] S. Schmiechen, P. Pust, P. J. Schmidt, W. Schnick, *Nachr. Chem.* **2014**, 62, 847–851.
- [25] P. Pust, F. Hintze, C. Hecht, V. Weiler, A. Locher, D. Zitnanska, S. Harm, D. Wiechert, P. J. Schmidt, W. Schnick, *Chem. Mater.* **2014**, 26, 6113–6119.
- [26] P. Pust, V. Weiler, C. Hecht, A. Tücks, A. S. Wochnik, A.-K. Henß, D. Wiechert, C. Scheu, P. J. Schmidt, W. Schnick, *Nat. Mater.* **2014**, 13, 891–896.
- [27] E. Elzer, P. Strobel, V. Weiler, P. J. Schmidt, W. Schnick, *Chem. Mater.* **2020**, 32, 6611–6617.
- [28] C. Braun, *Bulk Materials of Doped Multinary Nitrides and Nitridosilicates, Their Production Method and Uses*, **2020**, EP20186968.
- [29] C. Braun, L. Mereacre, Z. Chen, A. Slabon, *ChemRxiv* **2020**, DOI 10.26434/chemrxiv.13473642.v1.
- [30] Y. Q. Li, N. Hirosaki, R. J. Xie, T. Takeda, M. Mitomo, *J. Lumin.* **2010**, 130, 1147–1153.
- [31] Q. Li, C. Gong, X. Cheng, Y. Zhang, *Ceram. Int.* **2015**, 41, 4227–4230.
- [32] Z. Huang, Z. Wang, H. Yuan, J. Zhang, F. Chen, Q. Shen, L. Zhang, *J. Mater. Sci.* **2018**, 53, 13573–13583.
- [33] L.-W. Yin, Y. Bando, Y.-C. Zhu, Y.-B. Li, *Appl. Phys. Lett.* **2003**, 83, 3584–3586.
- [34] R. Su, Z. F. Huang, F. Chen, Q. Shen, L. M. Zhang, in *Key Eng. Mater.*, Trans Tech Publications Ltd, **2017**, pp. 635–641.
- [35] X. Xu, T. Nishimura, Q. Huang, R.-J. Xie, N. Hirosaki, H. Tanaka, *J. Am. Ceram. Soc.* **2007**, 90, 4047–4049.
- [36] Z. Huang, F. Chen, Q. Shen, L. Zhang, *RSC Adv.* **2016**, 6, 7568–7574.
- [37] Z. Huang, F. Chen, R. Su, Z. Wang, J. Li, Q. Shen, L. Zhang, *J. Alloys Compd.* **2015**, 637, 376–381.
- [38] Z. Huang, R. Su, H. Yuan, J. Zhang, F. Chen, Q. Shen, L. Zhang, *Ceram. Int.* **2018**, 44, 10858–10862.
- [39] N. Liu, J. Zhang, Y. Duan, X. Li, S. Dong, *J. Eur. Ceram. Soc.* **2020**, 40, 1132–1138.
- [40] P. F. Becher, G. S. Painter, N. Shibata, S. B. Waters, H.-T. Lin, *J. Am. Ceram. Soc.* **2008**, 91, 2328–2336.
- [41] G. S. Painter, F. W. Averill, P. F. Becher, N. Shibata, K. Van Benthem, S. J. Pennycook, *Phys. Rev. B - Condens. Matter Mater. Phys.* **2008**, 78, 214206.
- [42] G. S. Painter, P. F. Becher, W. A. Shelton, R. L. Satet, M. J. Hoffmann, *Phys. Rev. B - Condens. Matter Mater. Phys.* **2004**, 70, 144108.
- [43] N. Shibata, G. S. Painter, R. L. Satet, M. J. Hoffmann, S. J. Pennycook, P. F. Becher, *Phys.*

*Rev. B - Condens. Matter Mater. Phys.* **2005**, 72, 140101.

- [44] H. Gu, X. Pan, R. M. Cannon, M. Rühle, *J. Am. Ceram. Soc.* **1998**, 81, 3125–3135.
- [45] H. Hayashi, K. Hirao, M. Toriyama, S. Kanzaki, K. Itatani, *J. Am. Ceram. Soc.* **2001**, 84, 3060–3062.
- [46] N. Shibata, S. J. Pennycook, T. R. Gosnell, G. S. Painter, W. A. Shelton, P. F. Becher, *Nature* **2004**, 428, 730–733.
- [47] J. a. Kechele, O. Oeckler, F. Stadler, W. Schnick, *Solid State Sci.* **2009**, 11, 537–543.
- [48] S. Shimooka, K. Uheda, M. Mikami, N. Kijima, H. Imura, K. Horibe, *WO088966* **2007**, A1.
- [49] Y. Q. Li, G. De With, H. T. Hintzen, *J. Electrochem. Soc.* **2006**, 153, DOI 10.1149/1.2167950.
- [50] Y. Q. Li, G. de With, H. T. Hintzen, *J. Alloys Compd.* **2004**, 385, 1–11.
- [51] M. J. Hoffmann, *Personal Message*, **2020**.
- [52] C. Braun, L. Mereacre, W. Hua, T. Stürzer, I. Ponomarev, P. Kroll, A. Slabon, Z. Chen, Y. Damour, X. Rocquefelte, J. Halet, S. Indris, *ChemElectroChem* **2020**, 7, 4550–4561.
- [53] D. H. Kim, J. H. Ryu, S. Y. Cho, *Appl. Phys. A Mater. Sci. Process.* **2011**, 102, 79–83.
- [54] Y. Q. Li, A. C. A. Delsing, G. De With, H. T. Hintzen, *Chem. Mater.* **2005**, 17, 3242–3248.
- [55] V. Bachmann, T. Jüstel, A. Meijerink, C. Ronda, P. J. Schmidt, *J. Lumin.* **2006**, 121, 441–449.
- [56] D. Halmurat, T. Yusufu, Q. Wang, J. He, A. Sidike, *Sci. Rep.* **2019**, 9, 14637.
- [57] R. Mueller-Mach, G. O. Mueller, in (Eds.: H.W. Yao, I.T. Ferguson, E.F. Schubert), *International Society For Optics And Photonics*, **2000**, pp. 30–41.
- [58] P. A. M. Berdowski, J. van Herk, L. Jansen, G. Blasse, *Phys. status solidi* **1984**, 125, 387–391.
- [59] P. Dorenbos, *J. Mater. Chem.* **2012**, 22, 22344–22349.
- [60] A. Ziegler, J. C. Idrobo, M. K. Cinibulk, C. Kisielowski, N. D. Browning, R. O. Ritchie, *Interface Structure and Atomic Bonding Characteristics in Silicon Nitride Ceramics*, **2004**.
- [61] T. Mizoguchi, I. Tanaka, *Phys. Rev. B - Condens. Matter Mater. Phys.* **2000**, 61, 2180–2187.
- [62] T. M. Tolhurst, P. Strobel, P. J. Schmidt, W. Schnick, A. Moewes, *Chem. Mater.* **2017**, 29, 7976–7983.
- [63] M. R. Amin, P. Strobel, A. Qamar, T. Giftthaler, W. Schnick, A. Moewes, *Adv. Opt. Mater.* **2020**, 8, 2000504.
- [64] T. de Boer, T. D. Boyko, C. Braun, W. Schnick, A. Moewes, *Phys. status solidi - Rapid Res. Lett.* **2015**, 9, 250–254.

- [65] M. R. Amin, E. Elzer, W. Schnick, A. Moewes, *J. Phys. Chem. C* **2021**, *125*, 11828–11837.
- [66] A. Lasia, in *Electrochem. Impedance Spectrosc. Its Appl.*, Springer New York, New York, NY, **2014**, pp. 251–255.
- [67] R. O’Hayre, M. Nanu, J. Schoonman, A. Goossens, *J. Phys. Chem. C* **2007**, *111*, 4809–4814.
- [68] K. Gelderman, L. Lee, S. W. Donne, *J. Chem. Educ.* **2007**, *84*, 685–688.
- [69] B. Iandolo, H. Zhang, B. Wickman, I. Zorić, G. Conibeer, A. Hellman, *RSC Adv.* **2015**, *5*, 61021–61030.
- [70] D. W. Hwang, J. Kim, T. J. Park, J. S. Lee, *Catal. Letters* **2002**, *80*, 53–57.